

# Relativistic Heavy–Ion Collisions in the Dynamical String–Parton Model

D. E. Malov, A. S. Umar, D. J. Ernst

*Department of Physics and Astronomy, Vanderbilt University, Nashville, TN 37235*

D. J. Dean

*Physics Division, Oak Ridge National Laboratory, Oak Ridge, TN 37831–6373*

(April 26, 2024)

We develop and extend the dynamical string parton model. This model, which is based on the salient features of QCD, uses classical Nambu-Goto strings with the endpoints identified as partons, an invariant string breaking model of the hadronization process, and interactions described as quark-quark interactions. In this work, the original model is extended to include a phenomenological quantization of the mass of the strings, an analytical technique for treating the incident nucleons as a distribution of string configurations determined by the experimentally measured structure function, the inclusion of the gluonic content of the nucleon through the introduction of purely gluonic strings, and the use of a hard parton-parton interaction taken from perturbative QCD combined with a phenomenological soft interaction. The limited number of parameters in the model are adjusted to  $e^+e^-$  and  $p-p$  data. Utilizing these parameters, the first calculations of the model for  $p-A$  and  $A-A$  collisions are presented and found to be in reasonable agreement with a broad set of data.

25.75.+r, 12.38.Mh

## I. INTRODUCTION

Relativistic heavy-ion collisions at sufficiently high energies offer the unique opportunity to probe highly excited dense nuclear matter under controlled laboratory conditions. The ultimate objective [1] of the field of relativistic heavy-ion physics is to produce, detect, and study the properties of the quark gluon plasma (QGP), a new state of matter characterized by a transition to a phase of deconfined quarks and gluons. The fundamental confining property of the quantum chromodynamic (QCD) vacuum means that the deconfined state of a QGP is not directly observable. What is observable are hadronic and leptonic residues produced from the transient QGP state. In order to connect the properties of a QGP with experimental data from real nuclear collisions, theoretical models of these very complex, non-equilibrium collisions are needed. It is important that a variety of models be developed as no single model can hope to be complete in its ability to describe the system; each will have its strengths and limitations. We here develop and present results from the dynamical string-parton (DSP) model, a model which has as one of its strengths the detailed description of the interaction in time, from the initial state of two colliding nuclei through until the freeze-out of all the produced final-state particles.

The string-parton model [2–5] is a fully dynamical but classical string picture of hadrons and their collisions. The model incorporates both confinement and asymptotic freedom. In this model, the classical equations of motion for covariant strings determines the motion of hadronic matter according to the Lagrangian proposed by Nambu and Gotō [6]. The string is viewed as a gluon field with massless quarks attached at its endpoints. Mesons have a quark at one end and an antiquark at the other, while baryons have a diquark at one end and a quark at the other. Colliding strings interact via quark and gluon interactions. A covariant and causal hadronization mechanism for the strings is included in the form of a dynamic, probabilistic, and invariant scheme for the decay of excited strings [3]. The distinction of this model from others is the inclusion of both real-time dynamical string evolution as well as the inclusion of quark and gluon scattering as the sole source of the hadronic interactions. The model is minimalist and completely dynamic. Once the parameters of the string breaking and the quark and gluon interactions are fixed, collisions are studied by evolving the string equations of motion in three-space and one-time dimensions. The model produces quite well the average properties of a broad scope of reactions, including  $e^+e^-$ , hadron-hadron [3], lepton-nucleus [4], and nucleus-nucleus collisions [5].

The string-parton model is different in some essential ways from models based on the ideas of the classical string that use collision generator concepts, the (LUND [7], FRITIOF [8], RQMD [9], and QGSM [10]) models. The strings in the DSP model are not longitudinal; they are evolved according to the dynamics of the underlying Lagrangian. In comparison to other approaches, the string parton model is also quite minimalist. Fragmentation in most models is a process that involves a variety of terms each with its own flavor-dependent parameters. The decay scheme developed here is much simpler and flavor independent; flavor enters through the quantization [11] of the final-state hadronic masses. The differences between the models are motivated by the intended applications of the model. Since the DSP model describes reactions by calculating explicitly the time evolution of the participant strings, we are limited in the complexity of the fragmentation model that we are able to employ. In the DSP model, the few parameters needed to describe fragmentation are determined from  $e^+e^-$  reactions [11]. Quark-quark, quark-gluon, and gluon-gluon interactions are introduced and adjusted to fit the basic features of  $p-p$  collisions. At the  $p-A$  and nucleus-nucleus level, the model is completely predictive.

In the next section, we review the original model and some already published refinements that we have made to that model. In the original model, all mesons were treated as one generic meson of mass about 240 MeV. The model was not capable of addressing data in which the final state mesons were specifically identified. A technique has been developed to quantize the masses of the mesons [11]. This together with a review of how the string configurations which make up the nucleon are determined from the experimentally measured structure function [12] is presented in Section II. In section III the model is further developed by 1) extending the model of the nucleon to include gluonic strings, thus incorporating the experimentally measured gluonic content of the nucleon into the model, and 2) extending the quark-quark, quark-gluon, and gluon-gluon interactions to contain both a hard process taken from perturbative QCD and a soft process that is determined phenomenologically. Also in Section III, we determine some of the limited number of parameters in the model from  $e^+e^-$  data. In Section IV, we examine  $p-p$  collisions where we find further constraints on the parameters and demonstrate the ability of the model to describe hadron-hadron

collisions. In Section V we present the first results for  $p$ - $A$  collisions of the new model, and in Section VI give the first results for  $A$ - $A$  collisions. Finally we summarize what we have learned from the model and provide thoughts on future work, both applications and possible improvements and generalizations.

## II. NEW ENHANCED MODEL

In this section we review the model and several enhancements to the model — these include a new analytic method [12] for determining the distribution of string solutions that make up a nucleon directly from the experimentally measured structure function and the method [12] for quantizing the masses of the mesons. These have been published elsewhere. The first results for hadronic collisions which employ these enhancements are presented here in Sections III, IV, and V.

The classical Nambu-Gotō Lagrangian [6] provides a covariant description of the motion of a classical string with massless endpoints. The Lagrangian is defined as proportional to the invariant area swept out by the string,

$$S = -\kappa \int dA = -\kappa \int_{\tau_i}^{\tau_f} \int_0^{\sigma_f} \left\{ \left( \frac{\partial x^\mu}{\partial \sigma} \frac{\partial x_\mu}{\partial \tau} \right)^2 - \left( \frac{\partial x}{\partial \sigma} \right)^2 \left( \frac{\partial x}{\partial \tau} \right)^2 \right\}^{\frac{1}{2}}, \quad (1)$$

where  $\sigma$  and  $\tau$  are parametric variables that determine the location of the point  $x^\mu(\sigma, \tau)$ , where  $x^\mu(\sigma, \tau)$  is a point which lies on the area swept out by the string. The usual continuum mechanics algebra produces the equations of motion for the string. The proportionality constant  $\kappa$  is a parameter of the model and has units of energy/length. It is called the string constant and determines the scale at which the space-time evolution occurs. It is a parameter of the model. Lattice gauge calculations [13] produce the linear potential between quarks implied by this Lagrangian. For strings with total momentum zero, the solutions to the Lagrangian are characterized by a closed trajectory. For each trajectory, the endpoints of the string travel around the closed trajectory at the speed of light. The location of the string connecting the endpoints follows from the equations of motion. To obtain strings with non-zero momenta, the stationary strings are simply boosted relative to their rest frame.

For each trajectory, the endpoints of the string carry a finite and well determined fraction of the energy and momentum of the string. We identify these endpoints as quarks [3]. As the endpoints move at the speed of light, they represent massless quarks. For mesons, the endpoints are taken to be a quark and anti-quark; for nucleons, the endpoints are identified with a quark and a di-quark. The electromagnetic structure function provides an experimental measure of the longitudinal momentum fraction  $x$  carried by the quarks, with  $x$  defined by

$$x = \frac{k_0 + k_3}{P_0 + P_3}, \quad (2)$$

where  $k_0$  and  $k_3$  ( $P_0$  and  $P_3$ ) are the energy and  $z$ -component of the quark's (whole string's) momentum. For any string trajectory, the momentum fraction carried by the quarks can be calculated by averaging over the orientation of the string and over both one complete period

of motion, and finally taking the limit to the infinite momentum frame. Each trajectory thus implies a particular result for the structure function. Turning this around, we use the experimentally measured structure function of a hadron to determine a distribution of trajectories that will reproduce the experimentally measured results. This concept of utilizing a distribution of trajectories of classical strings to model the structure function is used here and has also been applied in Ref. [14]. In Ref. [12] this concept was pushed one step further. There it was shown that the structure function can be analytically related to the distribution of straight line segments making up the trajectories, assuming that trajectories are polygons made up of straight line segments. The results of these calculations demonstrate that the nucleon can be modeled as strings with a large number of straight line segments — a significant fraction of the distribution is for strings with greater than ten segments. The nucleon has no probability [12] of being a one-segment or one-dimensional solution. In this one-segment solution, the quarks oscillate back and forth along a straight line, a solution which is called the *yo-yo*. The structure function for the yo-yo solution can be calculated analytically [12,15]. The yo-yo is the only shape which contributes in the limit  $x \rightarrow 1$ . For this solution, and this solution only, the probability of one quark carrying all the momentum goes to zero linearly in  $1 - x$ . For the three-quark nucleon it is not surprising that this solution is absent. For the two-quark pion, however, there is a finite probability for the pion to be a yo-yo, or nearly so. Many models, however, are based on or are motivated by the yo-yo solution to the classical string model.

The results of Ref. [12] provides a means for initializing the proton as a distribution of strings with the correct parton momentum distribution. The analytical results are supplemented by a prescription which randomly attaches the calculated distribution of straight line segments to form closed trajectories. This collection of strings then forms the nucleon. A moving nucleon results from boosting the collection of strings from the rest frame. This provides the needed model of an incident nucleon, and, by distributing nucleons according to their experimentally measured spatial and momentum distribution in a nucleus, a model of an incident nucleus. Note that the model of the nucleon/nucleus is completely determined by experimental data other than the hadronic reactions which are to be studied. We must also supplement the dynamics by interactions and decays.

A model of the hadronization process is necessary if we are to model high-energy nuclear processes. The hadronization process is believed to take place via soft non-perturbative mechanisms. The DSP model assumes that an excited and therefore stretching color flux-tube breaks via the creation of a  $q\bar{q}$  pair with the color field of the new pair equal and opposite that found in the parent string. A covariant description [3] results from assuming that the probability of a string breaking is proportional to the invariant area,  $\delta A$ , swept out by the string,

$$\delta\mathcal{P} = \Lambda \delta A . \tag{3}$$

The proportionality constant  $\Lambda$  is a parameter to be determined from experimental data. It determines the rate at which strings break and thus will be intimately related to the multiplicity of a reaction as well as other experimentally measurable quantities. This decay law is invariant because it is defined in terms of an invariant area, and it is causal as the breaking occurs at a single point on the string. The probability that a string which is present at time  $t_1$  will survive until time  $t_2$  is then the exponential

$$\mathcal{P}(t_1 \rightarrow t_2) = \exp(-\Lambda A(\delta t)) , \quad (4)$$

where  $\delta t = t_2 - t_1$ .

Hadronization is then treated stochastically. As a string evolves in time, it decays according to the probability given by Eq. (4). If a string is to decay, it breaks at a point chosen randomly along its length. We have examined the possibility of calculating the tension locally along the string and then having the string break at each point according to the tension at that point. We found that this possible refinement had no significant impact on experimentally measurable quantities, so we do not utilize it.

Much of the qualitative features of hadronization are contained in this simple model:

- The intuitive picture of a string breaking more often the more it is stretched is built in. The more highly excited the string, the more likely it will break since the string sweeps through more invariant area.
- The uniform distribution of pions and the rapidity plateau emerge naturally.
- The leading particle effect results from having those particles created in the central region arising from quark-quark interactions that produce highly excited strings which fragment first. String pieces arising from the primary quarks are less excited and fragment last.

This model presents a problem that is completely analogous to a problem with the classical Bohr model of the atom. In the Bohr model, the electron would continue to radiate until it spiraled into the nucleus. Here, a string would continue to decay until it became an infinite number of very small pieces each with very little energy. In the original DSP model [2–5], a generic meson mass was introduced. Meson strings were allowed to decay if they had sufficient energy to make two of these generic mesons. Otherwise, the string could not decay and was identified as a generic meson. For baryonic strings, strings with masses greater than the nucleon mass plus the generic meson mass were permitted to decay; the rest would be identified with the nucleon. This scheme is very limiting. It allowed the model to address questions of mass flow, momentum flow, and multiplicity, but could not address meson identification, as is common for contemporary experimental data.

The model was generalized [11] by quantizing the mass of the classical strings. This is done by creating mass windows, energy regions that extend from the physical meson mass,  $m_i$ , to the physical mass plus a small increment,  $\delta m_i$ . If the mass of a string created in a hadronization process lands within one of these windows, the point at which the string decays is adjusted a small amount to produce a section of string with a mass equal to the physical meson mass. Once a string is identified with a meson, it is no longer allowed to decay. Thus the mass of a string in the final state is quantized to be the mass of a physical meson (within the small width that results from the numerical discretization of the string). Strings with a mass larger than the heaviest meson (we take a cutoff of 1 GeV) are always allowed to decay, as are strings with masses that fall between the mass windows. Phase space arguments were provided that predict the width of each window  $\delta m_i$ . These results were found [11] to be in qualitative agreement with results that were obtained from fitting to meson multiplicities measured in  $e^+e^-$  experiments, as will be described in more detail in the next section.

A striking experimental feature of both the  $e^+e^- \rightarrow q\bar{q} \rightarrow$  hadrons reaction and the  $pp \rightarrow$  hadrons reaction is that the mean transverse momentum is always roughly  $\langle p_T \rangle \simeq 0.35$  GeV/c. This leads to the assumption that the production of low transverse momentum ( $p_T \leq 1.5$  GeV/c) in these experiments is due primarily to the fragmentation of the gluon field that binds the quarks. This can be modeled by giving the quarks created in a string breaking equal and opposite non-vanishing transverse momenta. Although the transverse cross-section comprises a small part of the total cross-section, it is of significant importance in relativistic heavy-ion collisions since it can be used as a measure of the *stopping* experienced by the nuclei [16]. Various models of  $q\bar{q}$  pair production [17] predict a Gaussian transverse momentum distribution during the string breaking, but this falls far short of the experimentally measured distributions. Extensions of such models to infinitely long, uniform color-electric flux-tubes with finite transverse size may be a remedy [18]. In the absence of any fundamental calculations, we chose to parameterize the transverse momentum acquired by the created quarks with a simple exponential distribution function

$$f(p_T)p_T dp_T \propto e^{-\alpha p_T} p_T dp_T . \quad (5)$$

The average experimental transverse momentum is approximately related to  $\alpha$  in Eq. (5) by  $\langle p_T \rangle = 2/\alpha$ . This is not an analytically exact relationship as the transverse direction to the string is not, particularly after a number of quark collisions, the same as the transverse direction in the reaction plane and because the high-momentum tail in Eq. (5) cannot occur as these momenta would violate conservation of energy-momentum.

The final ingredient needed to be able to model hadronic collisions is a model of the hadron-hadron interaction. In this work, we further refine the model of the hadronic interactions. This new model is developed in Section IV. We also modify the model of the nucleon so as to include the experimentally determined gluonic content of the nucleon into the model. This development is also given in Section IV. Preliminary results which contained some of these new elements developed here can be found in Refs. [15,19].

### III. HADRORIZATION AND ELECTRON-POSITRON COLLISIONS

In this section we describe our model of the hadronization process and how the parameters which control the process are determined from  $e^+e^-$  data. The simulation of an  $e^+e^-$  collision begins at the  $q\bar{q}$  vertex where a quark and anti-quark are created with oppositely directed momenta and move apart, stretching the string between them. The parameters that relate to the quark and gluon interactions are to be determined from  $p-p$  collisions which will be presented in the next section. However, we will also show here that the quark and gluon interactions play an important role in  $e^+e^-$  dynamics. This physics had been neglected in the previous version of the DSP model. The determination of the parameters of the model no longer separates into first using  $e^+e^-$  data to determine the hadronization parameters and then using  $p-p$  interactions to determine the interaction parameters. Instead, the best interaction parameters must be used while determining the hadronization parameters, and vice versa.

The first parameter is the string constant  $\kappa$  that sets the energy scale of the model. The Regge model of highly excited hadrons [20] pictures these states as rotational states built on

individual excited states. The string model also provides a picture of excited states arising from rotating strings and gives the linear trajectories found in the Regge model. The slope of these trajectories is the string tension and is found experimentally [20] to be  $\kappa = 0.88$  GeV/fm. We will utilize this value; thus this parameter is determined completely external to our model.

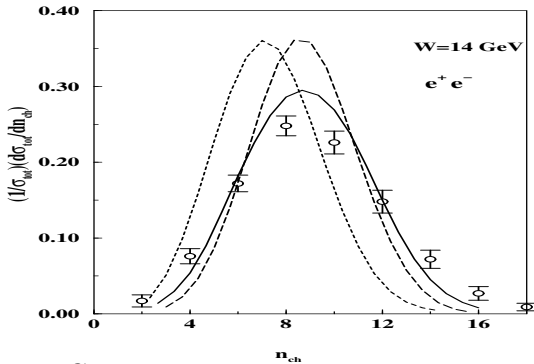


FIG. 1. Charged particle multiplicity distributions in  $e^+e^-$  collisions at  $\sqrt{s} = 14$  GeV. The data are from the TASSO experiment [21]. The solid line is the prediction of the SP model with the interaction of the quarks turned on and  $\Lambda = 1$ . The long-dashed curve corresponds to  $\Lambda = 1$  and the interaction of the quarks turned off. The short-dashed curve has the quark interaction turned on but with  $\Lambda = 4$ .

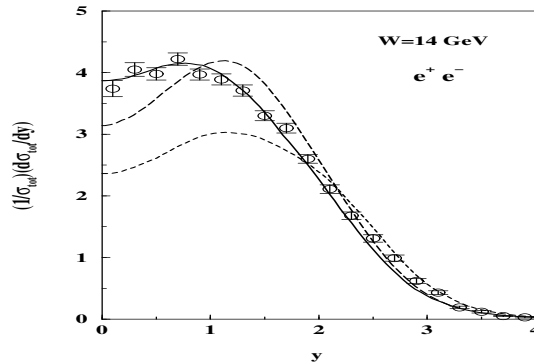


FIG. 2. The same as Fig. (1) except the rapidity distribution is presented.

The next parameter to be determined is the decay parameter  $\Lambda$  in Eq. (4). This parameter determines the rate at which excited strings decay and has a broad effect on measurable quantities in  $e^+e^-$  reactions. However, we have also discovered a new phenomena, the dynamics of the  $e^+e^-$  reaction are also affected by the quark and gluon interactions. In the next section we will describe, in detail, our model of these interactions. Here, we will demonstrate their effect on the  $e^+e^-$  theoretical results. To do this, we present calculations which utilize the best-fit parameters for the interactions from the next section to compare with results in which we neglect these interactions completely. In Fig. (1) we show the charged particle multiplicity distribution for  $e^+e^-$  collisions at 14 GeV. The data are from the TASSO collaboration [21]. We compare the solid line, the calculation with  $\Lambda = 1 \text{ fm}^{-2}$  and the rescattering between the created quarks included with the dashed line in which the rescattering is turned off. The average multiplicity is not changed by the rescattering; the peaks of the two curves are at the same value of the multiplicity. However, the rescattering broadens the curve and moves it much closer to the data. The effect of increasing  $\Lambda$  is to change the average as well as the width. This is illustrated by the short-dashed curve in Fig. (1). In Fig. (2) the rapidity  $y = (1/2) \log((E + p_l)/(E - p_l))$  distribution is shown, and in Fig. (3) the scaled longitudinal momentum  $x_f = 2p_l/\sqrt{s}$  distribution  $(1/\sigma_{tot})(d\sigma/dp_f)$  is shown. The curves are coded as in Fig. (1). We have found that including the rescattering of the created quarks is necessary if we are to fit these results. Notice that the rapidity distribution without the rescattering, the dashed curve in Fig. (2), has a peak between  $y = 1$  and  $y = 2$ . We have found this peak to be a persistent feature in all calculations which do

not include this additional rescattering. Similarly, the rescattering naturally enhances the fractional longitudinal momentum distribution near  $x_f = 0$ , as is needed in the data.

By looking at the parameters and assumptions of our model, we can understand why this additional scattering must be included. Upon breaking, the newly created endpoints of the string do *not* satisfy the energy-momentum relationship of an on-shell massless particle. They are virtual and have a mass deficit. These quarks proceed along the string absorbing the energy in the string until they have gained sufficient energy to come on the mass shell. In our model, the created quarks are assigned a longitudinal momentum equal to the created transverse momentum. This assignment is chosen as this will allow the quark to come on to the mass shell as quickly as possible. We have examined other assignments of longitudinal momentum during the string breaking, but the data seems to prefer this original choice. A part of our model is not to allow the quarks to interact until they are on-shell. This is motivated by the view that these interactions are mediated by gluonic exchanges. The propagator for the exchanged gluon would be suppressed if one of the interacting particles is highly virtual. We model this by not allowing the off-shell quarks and gluons to interact.

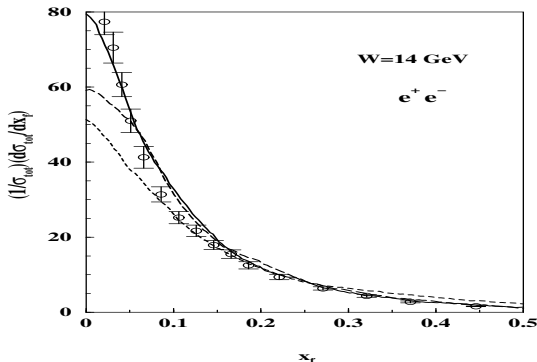


FIG. 3. The same as Fig. (1) except the fractional longitudinal momentum distribution is presented.

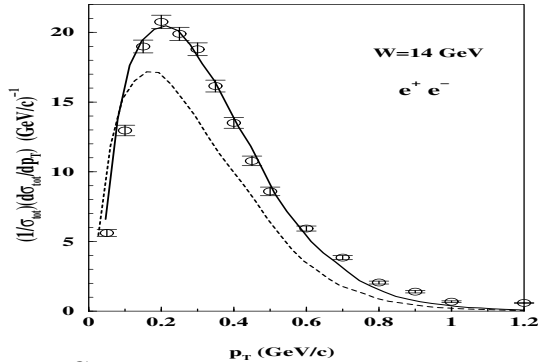


FIG. 4. The same as Fig. (1) except the transverse momentum distribution is presented. The curve with the quark interaction turned off is not presented because it produces results very near to the solid line.

The average transverse momentum created in a string breaking is related to  $\alpha$  in Eq. (5) approximately by  $\langle p_T \rangle = 2/\alpha$ . We will find that  $\alpha = 3.88 (GeV/c)^{-1}$ , a value determined by the experimentally measured low transverse momentum distributions in  $e^+e^-$  reactions. The time to come on shell is proportional to  $p_T$  in the rest frame of the created pair. The quarks will be of the order of  $2\langle p_T \rangle$  apart when they come on shell, or about 0.70 GeV/c. This is roughly equal to the interaction radius  $r_g$  for the quarks or gluons to interact. Thus one would expect a significant fraction of the created quark pairs to interact with each other after their creation.

Another way of viewing this is that the assignment of a transverse momentum (and an accompanying longitudinal momentum) at the string breaking is, itself, a model of the interaction of the created quark pairs. However, this model does not produce the experimental data. Without adding additional parameters to the model, but simply by making it more internally consistent, we find improved results, particularly for rapidity and  $x_f$  distributions.



We note that the quark-quark, quark-gluon, and gluon-gluon interactions will be found to have hard (high-momentum) and soft (low-momentum) contributions. The value of  $\alpha$  restricts the momenta of the created pair to a region where only the soft amplitude is effective in this rescattering.

In Figs. (1-3), we also show results with  $\Lambda = 4 \text{ fm}^{-2}$  (short-dashed curves) to compare with  $\Lambda = 1 \text{ fm}^{-2}$  (solid curve). The LUND model [7] gives a value of  $1 \text{ fm}^{-2}$ . In Fig. (4) we also show the transverse momentum distribution, with  $\alpha$  in Eq. (5) set equal to  $3.88 \text{ (GeV/c)}^{-1}$ . Quark rescattering has very little effect on the transverse momentum produced in the reaction so that curve is not shown in this figure. We see that a value for  $\Lambda$  near the LUND model value is required by the experimental data. Increasing  $\Lambda$  causes the strings to decay faster and hence reduces the multiplicity. Too low an average multiplicity then propagates through the other distributions giving results which are low for small rapidity, low for small fractional longitudinal momentum, and low for all but the smallest transverse momenta. We have not found a need to fine tune the value of  $\Lambda$ ; we use the value of  $1 \text{ fm}^{-2}$  suggested by the LUND model.

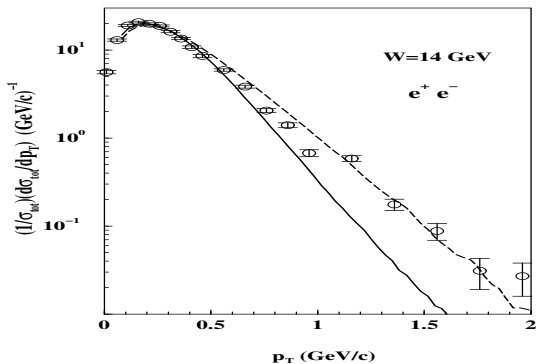


FIG. 5. Transverse momentum distributions in  $e^+e^-$  collisions at  $\sqrt{s} = 14 \text{ GeV}$ . The data are from the TASSO experiment [21]. The solid curve is for  $\alpha = 3.88 \text{ (GeV/c)}^{-1}$  and the dashed curve is for  $\alpha = 1.5 \text{ (GeV/c)}^{-1}$ .

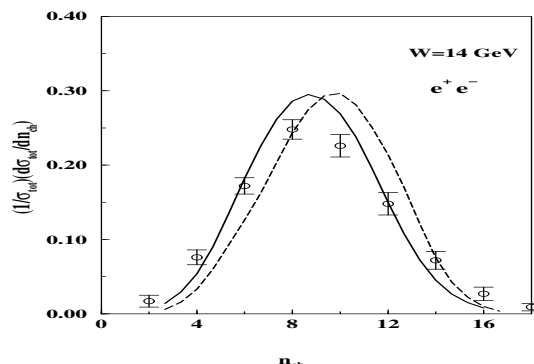


FIG. 6. The same as Fig. (5) except the multiplicity distribution is given.

The next parameter to be determined is the parameter  $\alpha$  in Eq. (5) — the parameter which governs the creation of transverse (to the string) momentum when a string breaks. This

TABLE I. The values of the windows  $\delta m_i$  for particles production identified in the model.

particle	particle mass (GeV)	$m_{min}$ (GeV)	$m_{max}$ (GeV)	reaction type
$\pi$	0.14	0.14	0.42	$e^+e^-$ , $pp$
$K$	0.49	0.49	0.63	$e^+e^-$ , $pp$
$p$	0.94	0.94	1.30	$e^+e^-$ , $pp$
$\eta$	0.54	0.63	0.68	$e^+e^-$
$\rho, \omega$	0.77	0.77	0.85	$e^+e^-$
$K^*$	0.89	0.89	0.98	$e^+e^-$
$\eta'$	0.96	0.98	0.99	$e^+e^-$
$f_0$	0.98	0.990	0.997	$e^+e^-$

parameter is clearly to be determined by the transverse momentum distribution in the  $e^+e^-$  reactions. We depict the normalized transverse momentum distribution  $(1/\sigma_{tot})(d\sigma/dp_T)$  in Fig. (5). The solid curve is for  $\alpha = 3.88 \text{ (GeV/c)}^{-1}$  and the long-dashed curve is for  $\alpha = 1.50 \text{ (GeV/c)}^{-1}$ . The data for  $p_T > 1 \text{ GeV/c}$  would prefer the latter value. However, the model does not include some physics, such as gluon bremsstrahlung. This missing piece of physics is believed to be the source of the very large  $p_T$  events as can be deduced from a change in the slope of the curve. Moreover, fitting the high energy tail of this reaction amounts to letting a very small fraction of the total events determine the value of  $\alpha$ . We believe the best approach is to fit, in detail, the peak of the  $p_T$  curve which constitutes the majority of the events. Under predicting the tail then leaves room to add other large momentum transfer physics which would increase the small number of very high-momentum particles and reproduce the tail of the distribution. We thus use the value of  $3.88 \text{ (GeV/c)}^{-1}$ . In Fig. (6) we show the multiplicity distribution for the two values of  $\alpha$ . Lowering  $\alpha$  from  $3.88 \text{ (GeV/c)}^{-1}$  (solid curve) to  $1.50 \text{ (GeV/c)}^{-1}$  has the effect of not only increasing the production of high momentum particles but also increases the average multiplicity, as would be expected. The multiplicity distribution further indicates that the preferred value of  $\alpha$  is  $3.88 \text{ (GeV/c)}^{-1}$ . We utilize this value and also find quite satisfactory results assuming  $\alpha$  is independent of the energy of the string. As noted in the previous section, we have developed [11] an approach to quantize the final state hadrons. The method consists of defining mass windows which extend from the physical mass of a meson  $m_i$  to  $m_i + \delta m_i$ . If, when a string breaks, one of the resulting segments has a mass which lies in the window, the string breaking point is adjusted slightly to produce a segment with the physical mass. Strings with the mass of a physical meson are then not allowed to decay. All other strings are allowed to continue to decay. Some special considerations must also be applied if the results would lead to a string that could not decay into two pions; the details are given in Ref. [11]. For the calculations we will present here, only the masses of the mesons are quantized. The baryonic strings are allowed to decay as long as the mass of a baryon is greater than the mass of the nucleon plus a pion. Strings with a mass smaller than this are identified as a nucleon and not allowed to decay. Windows for excited baryons can also be used when we wish to confront data in which excited baryons are to be specifically identified. It is important to realize that not allowing a string to decay does *not* mean the string will appear as a particle in the final state. The string will continue to interact, which will excite or de-excite it, after which it would continue through

TABLE II. Hadron multiplicities in  $e^+e^-$  annihilation events. The data are from [21] the TASSO collaboration; the theoretical results are labeled DSP Model.

$\sqrt{s}$ (GeV)	10	10	30	30
meson	TASSO	DSP Model	TASSO	DSP Model
$\pi$	9.8(0.5)	9.33	15.9(0.7)	16.08
$K$	1.81(0.09)	1.83	2.96(0.16)	2.92
$\eta$	0.20(0.04)	0.28	0.61(0.07)	0.49
$\rho, \omega$	0.65(0.12)	0.54	0.81(0.08)	0.90
$K^*$	0.56(0.06)	0.65	1.2(0.11)	1.01
$\eta'$	0.03(0.01)	0.049	0.26(0.1)	0.08
$f_0$	0.024(0.006)	0.032	0.11(0.04)	0.059

the regular decay process. The final state is dynamically determined when interactions cease to occur. The mass windows we find from fitting the  $e^+e^-$  data are given in Table I. We introduce windows and hence quantize the mass of the pion, kaon,  $\eta$ ,  $\rho$ ,  $\omega$ ,  $K^*$ ,  $\eta'$ , and  $f^0$ . However, when calculating results for hadronic collisions during the rest of this work, we utilize only the windows for the pion and kaon (and the proton) as the data we examine identify at most these three particles.

A stringent test of this model is to examine the production of individual mesons as a function of the energy of the  $e^+e^-$  collision. The mass windows are taken to be parameters that are independent of all other quantities. In Table II, we present the experimental results for pion, kaon,  $\eta$ ,  $\rho$ ,  $\omega$ ,  $K^*$ ,  $\eta'$ , and  $f^0$  production for energies  $\sqrt{s} = 10$  and 30 GeV. We see that the energy dependence is quite reasonably produced by this model.

#### IV. QUARK AND GLUON INTERACTIONS AND $P$ - $P$ COLLISIONS

Given the model of the nucleon and the model of hadronization presented in the previous section, we require only a model for the interaction of hadrons to be able to calculate hadronic collisions. In this section, we will present a model of the interaction between quarks and gluons, and describe a technique for incorporating the gluonic content of the nucleon into the model. These new features of the model incorporate more completely QCD phenomenology.

We have described the nucleon by a distribution of string solutions with the endpoints of each of the strings identified with a quark, anti-quark, or di-quark. However, evidence [22] indicates that a hadron contains a significant amount of glue. In particular, the momentum fraction of a hadron carried by the quarks as measured by deep inelastic scattering is [23] only 58% ( $Q = 1.6$  GeV) with an estimated error of 2%. The remaining momentum, 42%, we will assume is carried by the gluons. We will use this 58%-42% division in our simulations of proton-proton, proton-nucleus, and nucleus-nucleus collisions unless otherwise stated. For transverse energies  $E_T$  of jets produced in  $\bar{p}$ - $p$  collisions in the range  $50 \text{ GeV} < E_T < 450 \text{ GeV}$ , and  $x$  in the range of 0.06 – 0.5, the relative importance of the three subprocesses – quark-quark, quark-gluon, and gluon-gluon – shifts continuously from being gluon dominated to quark dominated [23]. This is also seen in the recent analysis of inclusive jet production cross section  $d\sigma/dE_T$  [24].

We wish to include in our model the significant gluonic content of the nucleon and the effect it will have on the hadronic collisions. In order to do this, we extend the model of the nucleon in terms of classical strings. In addition to the strings whose endpoints are identified as quarks, we will also include strings which we will identify as pure glue. The nucleon structure function is then divided between the contribution from the quarks and the contribution from the gluons, and is of the form

$$h(x) = C_q q(x) + C_g G(x) , \quad (6)$$

where the nucleon structure function is  $h(x)$ , its quark contribution  $q(x)$ , and gluon contribution  $G(x)$ , with probabilities  $C_q$  and  $C_g$ , respectively. A mathematical construction identical to the one given in Ref. [12] allows us to introduce purely gluonic strings and relate the distribution of their solutions to the measured gluonic structure function. For the gluon and quark structure functions, we utilized results from the Coordinated Theoretical/Experimental Project on QCD and Tests of the Standard Model (CTEQ) collaboration

[23]. We utilize the “modified minimal subtraction” model (also called  $\overline{\text{MS}}$  or CTEQ4M model) as it is described as “this set gives an excellent fit to all data sets” and “this set has the best overall quantitative agreement between the next to leading order QCD theory and the global data on high-energy scattering.” This model parameterizes the structure functions as,

$$q(x) = A_0 x^{A_1} (1-x)^{A_2} (1+A_3 x^{A_4}), \quad (7)$$

with the parameters [23] given in Table III. Next the model of the interaction between hadrons is described. We assume that hadrons interact via the interaction between the quarks, identified as the endpoints of the quark strings. In addition, we assume an analogous model for the interactions that involve gluonic strings. The interaction takes place between the endpoints of the gluonic strings that contain a finite fraction of the energy and momentum in the string. Thus we identify the endpoints of all strings as point like partons and model the interactions as parton-parton interactions.

In the parton model assuming factorization [22], the total cross-section for  $p$ - $p$  collisions is given in terms of the parton structure functions  $q(x)$ , and the elementary parton cross-sections by

$$\sigma_{pp} = \sum_{\alpha,\beta} \int dx_1 dx_2 d\Omega q_\alpha(x_1) q_\beta(x_2) \frac{d\sigma(q_\alpha q_\beta \rightarrow q_\alpha q_\beta)}{d\Omega}. \quad (8)$$

where  $C_q q(x_i)$  in Eq. (6) is the sum of the up and down quark structure functions  $q_\alpha(x_i)$  and  $C_g G(x_i)$  is the gluon structure function. Thus  $q_\alpha(x_i) dx_i$  is the probability of finding a parton of flavor  $\alpha$  with momentum fraction  $x_i$  in nucleon  $i$ , and  $d\sigma/d\Omega$  is the elementary scattering cross-section for the partons. If the parton scattering cross-sections are known, then the total hadronic cross-section can be calculated. Our model of the interaction of the partons allows them to interact if the partons from two different strings come within an interaction radius  $r_g$  of each other. Therefore, by considering a large number of  $p$ - $p$  collisions at fixed value of impact parameter  $b$  we can estimate scattering probability  $P(b)$  as ratio of reactions with interacting partons to the total number of reactions. This allows us to compute the total  $p$ - $p$  scattering cross section in the form

$$\sigma_{pp} = 2\pi \int_0^\infty P(b) b db. \quad (9)$$

Results of these calculations are shown in Fig. 7 for proton reactions simulated by quark strings and gluonic strings. Thus an interaction radius can be related to the [15,19]

TABLE III. Parameters in Eq. (7) for the CTEQ4M parton structure functions measured at  $Q_0 = 1.6$  GeV as taken from Ref. [23].

Parton	$A_0$	$A_1$	$A_2$	$A_3$	$A_4$	% Momentum
$xd_v$	0.640	0.501	4.247	2.690	0.333	11.2
$xu_v$	1.344	0.501	3.689	6.402	0.873	30.6
$xg$	1.123	-0.206	4.673	4.269	1.508	41.7

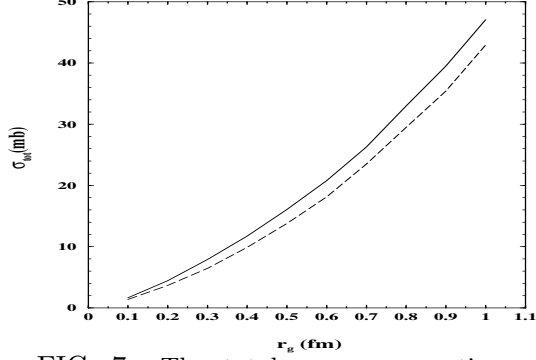


FIG. 7. The total  $p$ - $p$  cross-section as a function of  $r_g$ , the model parton-parton interaction radius, at  $\sqrt{s} = 30\text{GeV}$ . The solid curve assumes the proton is completely made up of quark strings, while the dashed curve assumes the proton is completely made up gluonic strings. The difference results from the different structure functions, as can be seen in Eq. (8).

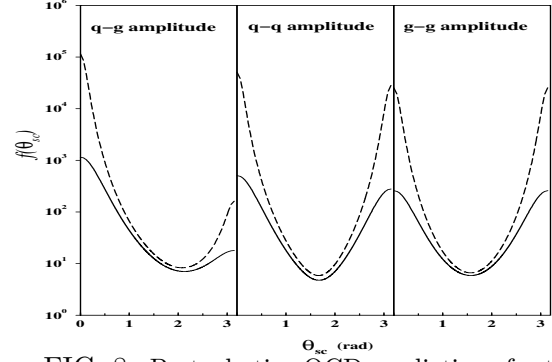


FIG. 8. Perturbative QCD predictions for the differential scattering cross sections for parton-parton (quark-gluon, quark-quark, gluon-gluon) scattering as a function of the center-of-mass scattering angle  $\theta_{sc}$  in radians. The solid curves are for a center-of-mass energy  $\sqrt{s} = 1\text{ GeV}$  while the dashed curves are for  $\sqrt{s} = 10\text{ GeV}$ .

experimentally measured  $p$ - $p$  total inelastic scattering cross section. An experimental total inelastic cross section of 28 mb [25], gives a parton interaction radius of  $r_g = 0.7\text{ fm}$  as pictured in Fig. 7. The solid curve is the result calculated assuming the proton is totally made up of quark strings while the dashed curve is the results assuming only gluonic strings. The difference arises from using the different structure functions, as would be expected from Eq. (8). We see that, although there is a difference between the curves, it is not large. This allows us to assume a single interaction radius for all of the parton-parton interactions, which, unless otherwise stated, will be taken as 0.7 fm.

As is conventional, we divided parton-parton scattering into two contributions, a soft part and a hard part. By definition, the hard part is taken directly from perturbative QCD calculations. We utilize the theoretical parton-parton cross-sections as given in Refs. [26,27]:

$$\frac{d\sigma}{d\hat{t}}(q_a q_b \rightarrow q_a q_b) = \frac{4\pi\alpha_s^2}{9\hat{s}^2} \left[ \frac{\hat{s}^2 + \hat{u}^2}{(\hat{t} - m_g^2)^2} + \delta_{ab} \left( \frac{\hat{t}^2 + \hat{s}^2}{(\hat{u} - m_g^2)^2} - \frac{2}{3} \frac{\hat{s}^2}{(\hat{u} - m_g^2)(\hat{t} - m_g^2)} \right) \right], \quad (10)$$

$$\frac{d\sigma}{d\hat{t}}(qg \rightarrow qg) = \frac{4\pi\alpha_s^2}{9\hat{s}^2} \left[ -\frac{\hat{u}}{(\hat{s} - m_g^2)} - \frac{\hat{s}}{(\hat{u} - m_g^2)} + \frac{9}{4} \left( \frac{\hat{s}^2 + \hat{u}^2}{(\hat{t} - m_g^2)^2} \right) \right], \quad (11)$$

$$\frac{d\sigma}{d\hat{t}}(gg \rightarrow gg) = \frac{9\pi\alpha_s^2}{2\hat{s}^2} \left[ 3 - \frac{\hat{t}\hat{u}}{(\hat{s} - m_g^2)^2} - \frac{\hat{s}\hat{u}}{(\hat{t} - m_g^2)^2} - \frac{\hat{s}\hat{t}}{(\hat{u} - m_g^2)^2} \right], \quad (12)$$

where  $\alpha_s^2 = g_s^2/(4\pi)$  and  $m_g$  is the gluon mass. The Mandelstam variables  $\hat{s}$ ,  $\hat{t}$  and  $\hat{u}$  for the massless quarks are given by  $\hat{s} = 2p_i \cdot p_j$ ,  $\hat{t} = -2p_i \cdot p_1 = -\hat{s}(1 - \cos\theta)/2$ , and  $\hat{u} = -2p_i \cdot p_2 = -\hat{s}(1 + \cos\theta)/2$ . These cross sections describe the scattering of two partons with incoming momentum states  $p_i$  and  $p_j$ , and outgoing momentum states  $p_1$  and  $p_2$ , and  $\theta$  is the angle between  $p_i$  and  $p_1$  as measured in the center-of-momentum frame of the partons.

We choose a gluon mass  $m_g = 0.25$  GeV which gives a range of the interaction consistent with the 28 mb  $p$ - $p$  inelastic cross-section.

For the hard interactions, we utilize the appropriate parton-parton scattering cross-sections given in Eqs. (10-12) and pictured in Fig. 8. If there is sufficiently large momentum transfer, then, as in deep inelastic scattering, the elementary interaction takes place very rapidly compared to the internal time scale of the hadronic interaction. In this case, the lowest order QCD predictions should describe the process. It is seen in Fig. 8 that these cross sections are forward and backward peaked. This forward and backward peaking is not present in proton-proton scattering, giving strong evidence that the momentum transfers are not generally large enough for the perturbative calculations to be valid.

At smaller momentum transfers, one would expect the interaction to be poorly modeled by perturbative QCD as the coupling constant  $\alpha$  becomes large [26] for small momenta, something seen in lattice QCD calculations [28]. We might expect the interaction to be dominated by a large number of non-perturbative soft gluon exchanges. Assuming incoherence in the collision process, the total momentum transfer would be a sum of many elementary momentum exchanges among the quanta of the color field,  $Q = \sum_j k_j$ . The transverse components of the  $k_j$ 's are in general rather small and pointing in random directions. Similar to a random walk in the transverse plane,  $Q$  would be expected to obey a Gaussian distribution with the average  $\langle Q \rangle$  on the order of the hadronic mass scale. However, the Gaussian distribution falls off too rapidly in comparison to data, so in our model we assumed for soft momentum transfers an exponential distribution,

$$f(Q) Q dQ \propto \exp(-\chi Q) Q dQ, \quad (13)$$

with the constant  $\chi$  of the order of an inverse hadronic mass scale. We utilize this single cross section for all the parton-parton soft interactions. Unfortunately it is very difficult to distinguish hadronic jets initiated by gluons from those initiated by quarks. Thus this minimalist assumption of equality of soft scatterings for the parton-parton interactions will not contradict any data and will be used unless or until we find a reason to assume otherwise.

We divide the parton-parton scattering into hard and soft events by introducing a threshold parameter  $\sqrt{\hat{s}_{min}}$ , where  $\sqrt{\hat{s}}$  is the center-of-mass energy of the two partons. If the center-of-mass energy of the interacting partons is greater than  $\sqrt{\hat{s}_{min}}$  then the partons interact via the hard interactions, Eqs. (10-12), and if the center-of-mass energy is less than  $\sqrt{\hat{s}_{min}}$  they interact via the soft interaction, Eq. (13).

To implement the hard and soft scattering cross sections numerically, we must scatter two partons whenever they come within a radius  $r_g$ . The scattering must obey the probability distributions implied by the differential cross sections given in the above formulae. For the hard scattering, we generate a random scattering angle chosen with a weight given by the appropriate cross section in Eqs. (10-12) and then numerically scatter the partons through the appropriate angle. For the soft scattering, we generate a random momentum transfer with a weight given by Eq. (13), calculate the corresponding scattering angle, and numerically scatter the partons through this angle. Proton-proton scattering is then simulated on the computer by generating a proton as a collection of strings chosen to reproduce the quark and gluon structure functions. A second proton is similarly generated. They are separated and boosted toward each other along trajectories with an impact parameter  $b$ . We evolve the strings according to their equations of motion and model the interactions of the

partons and the hadronization process as described above. Just as is done in an experiment, we count the number of final state particles, their energy and momentum, and construct the distributions which we wish to compare to experiment. The process is repeated by varying the impact parameter and by generating additional models of the proton, all constrained to provide on the average the exact experimental structure functions.

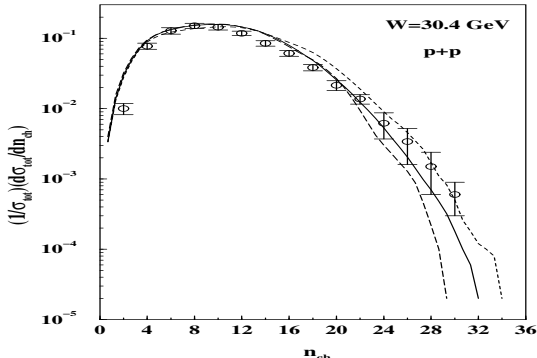


FIG. 9. Multiplicity distribution for  $p$ - $p$  collisions at  $\sqrt{s} = 30.4$  GeV. The data are from [25]. The long-dashed curve is the result assuming no hard parton-parton scattering, the solid line is the theoretical result with approximately 4% hard scattering and the remainder soft scattering according. The short-dashed curve results from a calculation in which approximately 19% is hard scattering.

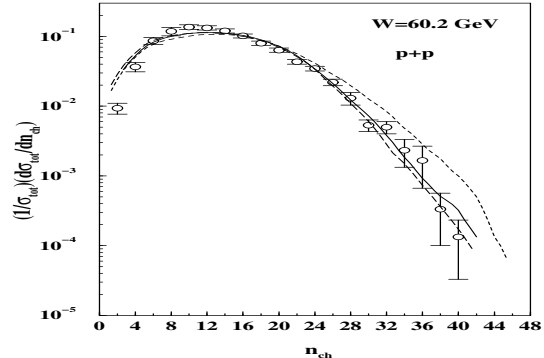


FIG. 10. The same as Fig. 9 except  $\sqrt{s} = 60.2$  GeV

From  $p$ - $p$  scattering we must determine the remaining parameters of the model. Intuitively, one would expect an increase in high multiplicity events with an increase in the amount of hard scattering. We find this to be true as depicted in in Figs. 9 and 10 where we show the experimental multiplicity [25] for  $p$ - $p$  collisions at  $\sqrt{s} = 30.4$  and 60.2 GeV. We use protons that are composed of 42% gluonic strings for these calculations. We also fix the soft momentum transfer parameter  $\chi$  in Eq. (13) to be  $0.7 \text{ fm}^{-1}$ . The long-dashed curves in both figures do not include any hard scattering. They fall rather close to the data indicating that the fraction of hard scattering is small. The short-dashed curve uses  $\sqrt{\hat{s}_{min}} = 2 \text{ GeV}$ . The percent hard scattering is then 18% at 30.4 GeV and 24% at 60.2 GeV. These curves produce too many high multiplicity events. We conclude that  $\sqrt{\hat{s}_{min}} = 4.0 \text{ GeV}$  which produces the solid curves. This corresponds to 4% at 30.4 GeV and 5% at 60.2 GeV of the scatterings being hard and reproduces quite well the high multiplicity tail. We conclude that hard scattering is not negligible but that it occurs only a small percent of the time.

We also need to determine the momentum transfer parameter  $\chi$  that governs the soft interaction, Eq. (13). In Fig. (11) the multiplicity distribution for  $p$ - $p$  scattering at  $\sqrt{s} = 30.4$  GeV is shown. The three curves represent three values for  $\chi$  —  $\chi = 0.4, 0.7,$  and  $1.0 \text{ fm}^{-1}$ . The inverse value of  $\chi$  corresponds to the average soft momentum transfer during the parton scattering. A decrease in the value of  $\chi$  causes an increase in the inelasticity of the process and therefore an increase in the multiplicity of the reaction, as can be seen in Fig. (11). We find that  $\chi = 0.7 \text{ fm}^{-1}$  gives the best fit, and utilize that value for our

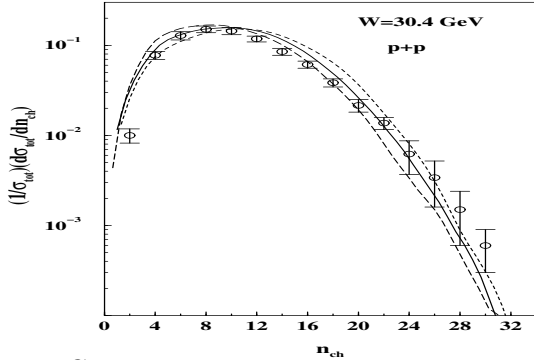


FIG. 11. Multiplicity distribution for  $p$ - $p$  collisions at  $\sqrt{s} = 30.4$  GeV. The data are from [25]. The long-dashed curve is a calculation with  $\chi = 1.0$ ; the solid line is  $\chi = 0.7$ , the value we choose for the model; and the short-dashed curve is the result with  $\chi = 0.4$

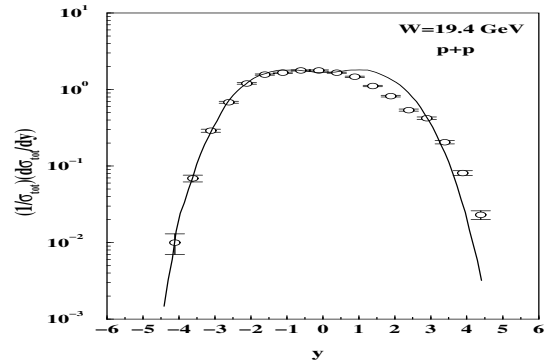


FIG. 12. Rapidity distribution for  $p$ - $p$  collisions at  $\sqrt{s} = 19.4$  GeV. The data are from [41] and the solid curve is the prediction of the DSP model developed here. The limited identification of protons leads to a distortion of the experimental rapidity distribution in the target hemisphere.

model. It is interesting to compare Fig. (9) with Fig. (11). The momentum transfer parameter  $\chi$  affects mostly the distribution near the peak multiplicity, while the amount of hard scattering affects mostly the tail of the distribution. We may also look at the experimental  $p_T$  distributions of the final state particles. The  $p_T$  distributions are to a good approximation exponential, at least over the range  $p_T = 0.1$  to  $1.1$  GeV/c [29]. We present in Table IV the slope parameters extracted from the data [30] and those calculated from our model. We take the fraction of the proton that is composed of gluon strings [22] to be 42% as extracted from data. However, it is interesting to ask whether this affects the calculated  $p$ - $p$  results. We also present in Table IV the slope parameters extracted from  $p_T$  distributions calculated using protons composed totally of quark strings and totally of gluon strings. We see that mixed state of 58% quark and 42% gluon content in the proton gives a better fit to data and indicates that significant fraction of the strings should be gluonic.

For completeness we also present in Fig. (12) the measured rapidity distribution for  $p$ - $p$  collisions at  $\sqrt{s} = 19.4$  GeV. The data are from Ref. [39]. The calculation utilizes our final choice for all of the parameters. These are given in Table V with a description of how they were determined. These results are completely predictive as this data was not used in determining any of the parameters. Notice the excellent results for negative rapidity. Also note that the experimental results are not symmetric as they must be.

TABLE IV. Slope parameters for the  $p_T$  distributions of the final state pions, kaons and protons in  $p$ - $p$  collisions at  $\sqrt{s} = 30.4$  GeV. The experimental values are from Ref. [30]. The results of calculations using the DSP model are presented, each using a different fraction, as labeled, of quarks versus gluons in the composition of the nucleon.

Particle	Slope $((GeV/c)^{-1})$	Slope $((GeV/c)^{-1})$	Slope $((GeV/c)^{-1})$	Slope $((GeV/c)^{-1})$
	Experiment	58%quark/42%gluon	100% quark	100%gluon
Pions	6.5-7.0	6.70	6.34	7.58
Kaons	5.0	4.97	4.62	6.46
Protons	4.0	4.12	3.70	5.79



This is a fixed target experiment and it is noted that for the positive rapidity region there was less than complete separation between pions and protons. We are thus very satisfied with the excellent results we find for negative rapidity, and discrepancies are largely a result of experimental distortion [39]. We describe the model as minimalist because the number of parameters is quite small in comparison to other models. In addition, once these parameters have been determined from  $e^+e^-$  and  $p-p$  collisions, the model is completely predictive. In the next section we describe how we construct a nucleus out of a distribution of nucleons. A  $p-A$  or  $A-A$  collision is then modeled by constructing the appropriate initial state, evolving it in time on the computer according to our covariant and dynamical model, and then collecting statistics on the final state particles, just as do the experimentalists.

## V. PROTON-NUCLEUS COLLISIONS

Proton-nucleus reactions are a definitive test of the string-parton model. The parameters of the model are completely determined from  $e^+e^-$  and  $p-p$  data. The model is now predictive and thus comparison to  $p-A$  and  $A-A$  data are a validation of the assumptions of the model, if the model compares well with the data.

Although the main focus of relativistic heavy-ion physics is on  $A-A$  collisions and the formation of the quark-gluon plasma,  $p-A$  provide an opportunity to study the dynamics of the hadronic interaction in a situation that is simpler than an  $A-A$  collision. As QCD is not capable of confronting this data, models are necessary. In order to create the densities and temperatures to form the plasma, a nucleon in one nucleus must collide multiple times with other nucleons and deposit a large amount of energy in the interaction region. The evidence of the occurrence of multiple collisions comes directly from experimental investigations [36]. The  $p-A$  system provides insight into how these multiple collisions come about.

In the  $p-A$  system at high-energies the identity of the proton and the particles created from its excitation is, to a great extent, maintained throughout the collision. This is indicated experimentally by distributions having a peak tied to the kinematics of the incident proton. The model and the experimental data then provide insight into the importance of multiple collisions for the incident proton and on how the second and subsequent collisions are modified [8,9] by having undergone a previous collision. This modification is significant because a head-on collision of two protons can create a highly excited string which will then

TABLE V. Parameters in the DSP model, their value, and how they are determined. In addition the mass windows used to quantize the mesonic strings are given in Table I.

[thbp]

Symbol	Description	Method of determination	Value
$\kappa$	String tension	Regge slope	0.88 GeV/fm
$\Lambda$	String decay rate	$e^+e^-$ multiplicity data	$1.0 \text{ fm}^{-2}$
$\alpha$	$p_T$ production constant	$e^+e^-$ $p_T$ data	$3.88 (\text{GeV}/c)^{-1}$
$r_g$	parton interaction radius	$pp$ total cross-section	0.7 fm
$\chi$	soft-momentum transfer constant	$pp$ and $e^+e^-$ data	$0.7 (\text{GeV}/c)^{-1}$
$\sqrt{\hat{s}_{min}}$	energy threshold for hard scattering	$pp$ multiplicity data	4 GeV

collide again before it has had time to decay. This phenomenon is included quite naturally in the DSP model since the interactions occur between quarks and the strings are evolved and decay in space-time according to the Lagrangian and the invariant decay scheme. The ability to vary the target is then very useful as this variation changes the distance through the nuclear medium that the incident proton must travel. The second peak in the distribution occurs at kinematics that indicate an origin in the  $A$  nucleons of the ion. For this kinematic region, there are  $A$  particles with nearly equal momentum, i.e. within a Fermi momentum of each other, and thus multiple scatterings will be more significant. This still remains a simpler situation than occurs in an  $A$ - $A$  system and thus can provide additional insights into the dynamics. Other theoretical models do not seem to have published results for the  $p$ - $A$  data so we are not able to compare our results to theirs.

There is one last theoretical piece yet needed to model  $p$ - $A$  collisions. We need to generate a model for a nucleus containing  $A$  nucleons. We employ a Fermi-density distribution

$$\rho(r) = \frac{\rho_0}{1 + \exp[(r - c)/a_0]}, \quad (14)$$

with parameters  $a_0 = 0.55$  fm the thickness of the nuclear surface,  $c = 1.18A^{1/3} - 0.48$  fm the half-density radius, and  $\rho_0 \simeq 0.07$  fm $^{-3}$  the central density [35]. The nuclear volume is then populated with nucleons, each constructed as a distribution of strings as described earlier, with the probability density  $\rho(r)$  determining the distribution of the nucleons. However, two nucleons in the same nucleus are not allowed to be within an interaction range. If the Monte Carlo chooses a location such that the quarks that make up a proton would be interacting with other quarks, another position is generated until a location is found such that the nucleus will not be composed of particles scattering from each other and causing the nucleus to react with itself before the physical collision begins. The nucleon is then offset from the  $z$ -axis by an impact parameter  $b$  which is either fixed or distributed over a range with the weight  $2\pi b db$  and the proton and the nucleus are translated in the longitudinal direction such that they do not overlap. The nucleus and the proton are then boosted towards each other with the collision Lorentz factor  $\gamma$  to reach the energy of the reaction, and the time evolution proceeds via the string equations of motion.

We here apply the DSP model to minimum bias data [41] for  $p+S$  and  $p+Au$  collisions at 200 GeV per nucleon. The rapidity distributions of net nucleons for minimum bias  $p+S$  and  $p+Au$  [43] are shown in Figs. 13 and 14. The data are for net protons while our model does not distinguish between the proton and the neutron. To account for this difference we multiply the data in the target hemisphere,  $y < 0$ , by two for isoscalar (equal number of neutrons and protons) nuclei ( $p+S$ ) and by a factor of  $A/Z$  for other cases. This result in a factor of 2.5 for  $p+Au$  reaction. For the projectile hemisphere the data and the calculation are for one nucleon (here a proton) so this data is not multiplied by two. Thus the plots are not net protons, but net nucleons. The solid curves in these figures are the predictions of the DSP model.

Near midrapidity,  $y = 0$ , for both reactions the model and the data agree quite well. For the projectile hemisphere,  $y > 0$ , the results for sulfur, Fig. 13, show a possible and small discrepancy with the data as the largest two rapidity points lie slightly below the theory.

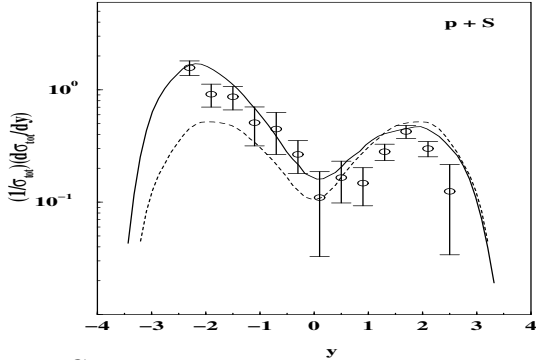


FIG. 13. Rapidity distribution of net nucleons for minimum bias  $p+S$  collisions at 200 GeV per nucleon. The data are from [41] and the solid curve is the prediction of the DSP model developed here. The dashed curve is the prediction of the DSP model for  $p-p$  collisions.

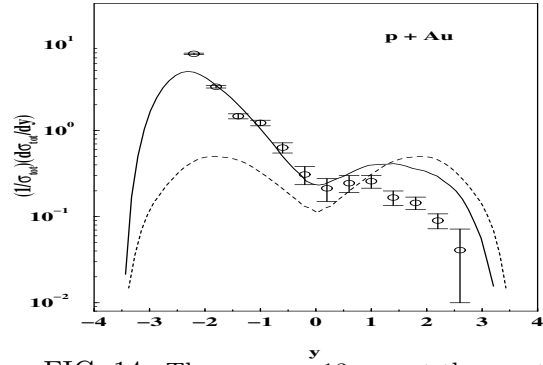


FIG. 14. The same as 13 except the reaction is  $p+Au$ .

The dashed curve in these figures represents the results of our model for  $p-p$  collisions. There is very little difference between the  $p-p$  collision curve and the  $p-A$  curve in this hemisphere. This indicates that for this kinematic region only a single proton scattering has occurred. As a check on our computer program, we restricted the calculation to a single nucleon scattering and found that we did indeed recover the  $p-p$  results pictured. If there is a discrepancy for the largest rapidity, its origin must be in the model of the  $p-p$  collision. For the gold target, the situation in the projectile hemisphere is very different. The data no longer show a distinct peak. This is a clear indication that there have been multiple collisions and significant stopping of the proton. The theory shows a broadened peak shifted to lower rapidity as compared to the  $p-p$  results (the dashed curve) indicating the existence of multiple scatterings. However, the theory is not producing as much stopping as is seen in the data. On the other hand, looking at the target hemisphere,  $y < 0$ , the data and the theory are quite compatible. Some caution must be made in drawing conclusions that make use of the lowest ( $y \leq -2.8$ ) and highest ( $y \geq 2.8$ ) rapidity points. These data [41] were extrapolated on the basis of a thermal fit. This was necessary because at low transverse momenta a cut was applied at 0.3 GeV. Also in comparing rapidity distributions for different systems one has to keep in mind that different forward energy triggers may affect the spectra differently [41]. In summary, we find satisfactory results except for the projectile hemisphere for the gold data, where the theory appears to underpredict the stopping of the incident proton.

The rapidity distributions of negatively charged hadrons produced in minimum bias  $p+S$  and  $p+Au$  collisions are shown in Figs. 15 and 16. The dashed curve is again the results of the DSP model for a nucleon-nucleon collision. In both the theory and the data, the multiplicity of negative hadrons increases with target mass and the maximum shifts to lower rapidities, indicating [41]  $\pi^-$  production after multiple collisions. We also see that the high rapidity  $y \geq 1.7$  region for  $p+S$  collisions is very near the  $p+p$  result indicating that this region is determined by a single scattering. Although the theory produces the very large enhancement for  $p-Au$  near  $y = -2$  over the  $p-p$  curve, the theory has a tendency to preserve a slight peak near the target rapidity that is not seen in the data.

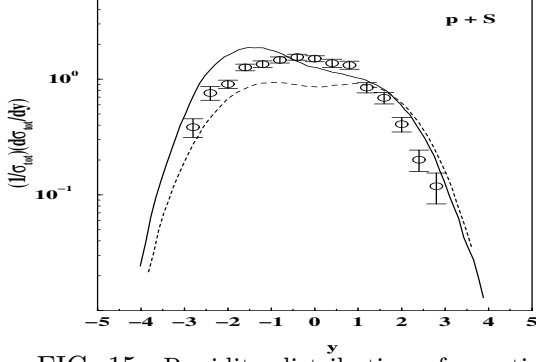


FIG. 15. Rapidity distribution of negatively charged hadrons for minimum bias  $p+S$  collisions at 200 GeV per nucleon. The data are from [41] and the solid curve is the prediction of the DSP model developed here. The dashed curve is the prediction of the DSP model for  $p-p$  collisions.

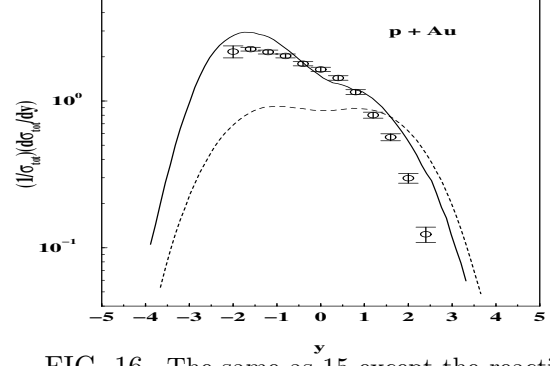


FIG. 16. The same as 15 except the reaction is  $p+Au$ .

The degree of thermalization in heavy-ion collisions and the possible effects of collective flow on the spectra can be studied by examining the transverse degrees of freedom. We calculate the spectra of protons, pions and kaons and compare to data from experiments NA35 and NA44 from CERN [41,44]. Figs. 17 and 18 show the transverse momentum distribution of net nucleons (scaled by a factor of two to represent nucleons rather than protons) for  $p+S$  and  $p+Au$  collisions at 200 GeV·A together with calculations of the DSP model. The calculations agree quite well with data.

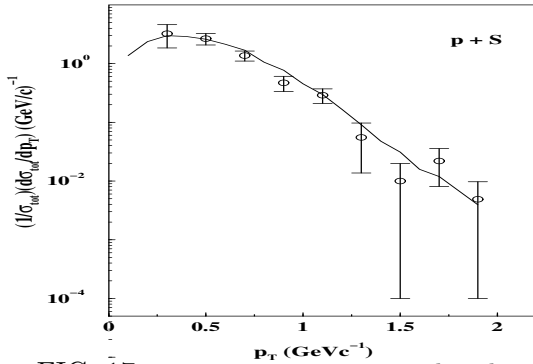


FIG. 17. Transverse momentum distributions of net nucleons for minimum bias  $p+S$  collisions at 200 GeV per nucleon. The data are from [41] and the solid curve is the prediction of the DSP model developed here.

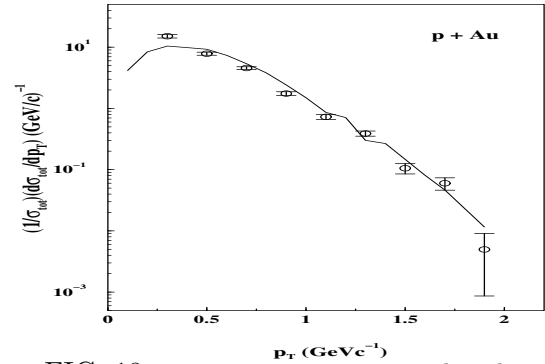


FIG. 18. Transverse momentum distributions of net protons for minimum bias  $p+Au$  collisions at 200 GeV per nucleon. The data are from [41] and the solid curve is the prediction of the DSP model developed here.

An inverse slope parameter (temperature) has been extracted from the data and can be calculated in our model. The results for protons, kaons, and pions are given in Table VI. We utilized data [44] for  $K^-$  in the midrapidity region  $k_T = \sqrt{p_T^2 + m_K^2} - m_K \leq 0.84 \text{ GeVc}^{-1}$  and for pions in the midrapidity region  $k_T = \sqrt{p_T^2 + m_\pi^2} - m_\pi \leq 0.64 \text{ GeVc}^{-1}$ . Very reasonable agreement is found for these parameters. In addition the pion spectra generated within the

model are not exponential for all values of  $m_T$ . They show an increase with increasing  $p_T$  which is also true of experimental data and other theoretical predictions [44–46]. We have found that the results of the model for  $p$ – $A$  collisions are often quantitatively in agreement with the data, but there exists in the net nucleon rapidity distribution for  $p$ – $Au$  an indication of more stopping of the incident proton in the data than is found in the theory. The rapidity distributions for negative hadrons would indicate a small increase in the hadronic interactions that would broaden the distribution of the produced hadrons. Other theoretical models have not published results for  $p$ – $A$  collisions so we cannot say how general these results might be. In comparison with the  $p$ – $p$  data, all of the general features found in the experiments in going to  $p$ – $A$  are contained in the theory. This gives us confidence that the model is capturing much of the important underlying physical phenomena.

## VI. NUCLEUS-NUCLEUS COLLISIONS

The spectra of produced particles and participant nucleons measured over a broad acceptance in rapidity  $y$  and transverse momentum  $p_T$  address many questions important to an understanding of the overall reaction dynamics. It is only in  $A$ – $A$  collisions that one would expect to create sufficient energy densities to create the QGP. Furthermore, in  $p$ – $A$  collisions it is difficult to disentangle the effects of rescattering of the spectator matter from the more interesting participant matter dynamics. In central  $A$ – $A$  collisions, the importance of rescattering among spectator matter is minimized and the dynamics of the highly excited, very dense, created matter becomes dominant.

As a first application to nucleus-nucleus collisions, the dynamical string-parton model is applied to the interaction  $S + S$  at 200 A GeV/c. The results of the calculations are to be compared to CERN data [41,42] for central S+S reactions. As was the case for  $p$ – $A$  collisions the calculations are completely predictive; all of the parameters of the model have been fixed by  $e^+e^-$  and  $p$ – $p$  data. In Fig. 19 the rapidity distribution for negatively charge hadrons is presented. For a pure prediction, this is a quite nice result. The theory predicts the midrapidity region quantitatively correctly. The only discrepancy is that the theory overpredicts the production of particles at the larger rapidity by a small amount. This could be a result of not having quite enough stopping in the theory. In Fig. 20 we show the rapidity distribution of net protons for the same reaction. The results are again quite good. There is not complete stopping for this reaction as two identifiable peaks remain, both in the data and in the theory. The theory does predict the absence of a sharp proton fragmentation peak and the filling of the midrapidity region.

TABLE VI. Slope parameters  $((GeV/c)^{-1})$  for the  $p_T$  distributions of the final state pions and kaons in  $p+S$  and  $p+Au(Pb)$  collisions at 200 GeV per nucleon. The experimental values are from Ref. [44].

Reaction	Pions	Kaons	Pions	Kaons
	Experiment (NA44)	Experiment (NA44)	DSP Model	DSP Model
$p + S$	$139 \pm 3$	$160 \pm 12$	135	141
$p+Au(Pb)$	$145 \pm 3$	$152 \pm 5$	142	145
$S + S$	$154 \pm 5$	$163 \pm 5$	147	143

The data would allow for a small increase in stopping which would fill in the midrapidity region slightly more, where the theory is within the error bars but is consistently low. We saw for  $p$ - $A$  collisions in Figs.13-16, particularly for  $p + Au$ , that the model was not producing quite as much stopping as is contained in the data. This is less noticeable here, but remains a consistent interpretation of the comparison of theory to data.

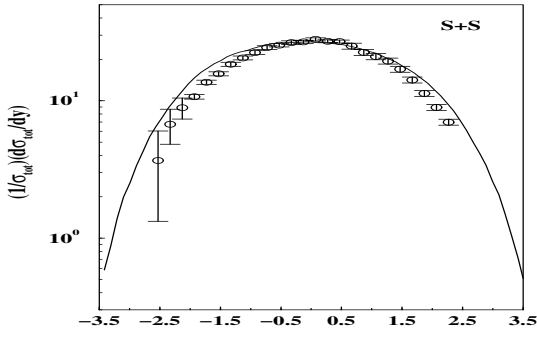


FIG. 19. Rapidity distribution of negatively charged hadrons for central  $S+S$  collisions at 200 GeV per nucleon. The data are from [41,42] and the solid curve is the prediction of the DSP model developed here.

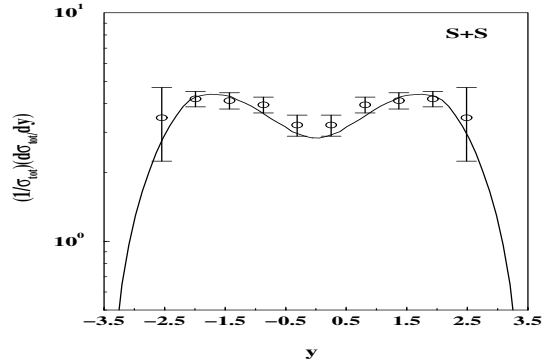


FIG. 20. Rapidity distribution of net protons for central  $S+S$  collisions at 200 GeV per nucleon. The data are from [41,42] and the solid curve is the prediction of the DSP model developed here.

In Fig. 21 we present the distribution of negatively charged particles for the collision  $Pb + Pb$  at 156 A GeV/c. The data [47] are from CERN. Comparing to the  $S + S$  results

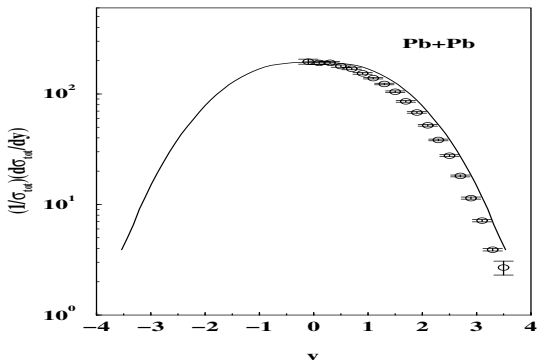


FIG. 21. Rapidity distribution of negatively charged hadrons for central  $Pb+Pb$  collisions at 156 GeV per nucleon. The data are from [47] and the solid curve is the prediction of the DSP model developed here.

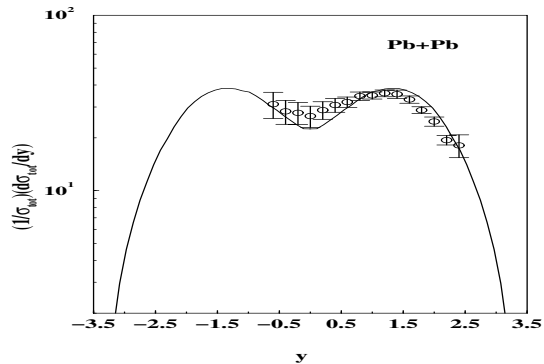


FIG. 22. Rapidity distribution of net protons for central  $Pb+Pb$  collisions at 156 GeV per nucleon. The data are from [47] and the solid curve is the prediction of the DSP model developed here.

in Fig. 19, the results are very comparable. The midrapidity,  $y = 0$ , value is predicted very well. For the largest rapidity, the theory is again overpredicting the experimental results but not by a large amount. In Fig. 22 the rapidity distribution of net protons for the  $Pb + Pb$  reaction is shown. Again, the results are very similar to what was found for  $S + S$  in Fig. 20. There is again incomplete stopping for this reaction as two identifiable peaks remain, both in the data and in the theory. The theory does predict the absence of a sharp proton fragmentation peak and the filling of the midrapidity region. Again, the data would allow

for a small increase in stopping which would fill in the midrapidity region somewhat more. In summary, the theoretical rapidity distributions for  $A$ - $A$  collisions at CERN energies are quite reasonable, but indicate that the model is slightly underpredicting the stopping.

In Fig. 23 we present the transverse momentum distribution of net protons for the  $S + S$  reaction at 200 A GeV/c and the experimental results from [41]. The theory is underpredicting somewhat the creation of transverse momentum for the protons. We present in

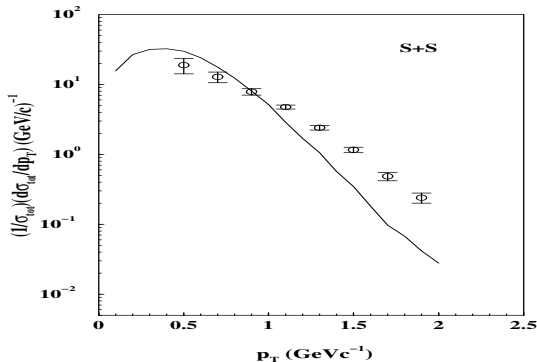


FIG. 23. Transverse momentum distributions of net protons for central  $S + S$  collisions at 200 GeV per nucleon. The data are from [41] and the solid curve is the prediction of the DSP model developed here.

Table VI the inverse slope parameters for transverse momentum distributions for pions and kaons. The reactions are  $p + S$ ,  $p + Au(Pb)$ , and  $S + S$  at 200 A GeV. In  $A$ - $A$  collisions, there is an increase in transverse momentum production in the data that is partially found in the theory. The experimental inverse slope parameter for pions produced in  $p + S$  collisions were found to be  $139 \pm 3$  MeV and  $145 \pm 3$  MeV for  $p + Au$ . The DSP model predicts 135 MeV and 142 MeV respectively, results that reasonably consistent. For  $S + S$  collisions the experimental inverse slope for pion production is  $154 \pm 5$  MeV while the DSP model prediction is 147 MeV, which is just outside the error bars. The transverse momentum production for kaons is consistently underpredicted by a small amount in the DSP model. The experimental inverse slopes are  $160 \pm 12$  MeV for  $p + S$  and  $152 \pm 5$  for  $p + Au$ . The theoretical results are 135 MeV and 142 MeV, respectively. Both of these theoretical numbers are somewhat small. For  $S + S$  collisions the inverse slope parameter for kaon production is  $163 \pm 5$  MeV for the data and 143 MeV for the DSP model. This data for kaon production for the  $S + S$  reaction indicates a rather large increase in the inverse slope over that for  $p+A$  collisions, something not found in the model.

## VII. CONCLUSIONS

In this paper, we further developed the string parton model of relativistic heavy-ion collisions of Ref. [2–5]. This dynamical model is based on Nambu-Gotō classical strings [6]. The strings evolve in time according to their covariant equation of motion and the endpoints of the string, which contain a finite amount of energy-momentum, are identified as quarks, antiquarks, or diquarks. Hadronization proceeds through a covariant and stochastic model of string breaking in which the probability of breaking is proportional to the invariant area swept out by the string. The quark-antiquark pair created at the point where the

string breaks acquire a transverse momentum taken from an exponential distribution. The interaction between particles is modeled as an elastic scattering between the massless quarks. Previous work [2–5] has found that the model reproduces quite well the average properties of  $p$ - $A$  and  $A$ - $A$  collisions.

In order to address more detailed properties of hadronic interaction data, we extended the model. First, the masses of the strings are phenomenologically quantized [11] to allow for particle identification in the final state. This is done by choosing windows such that if the invariant mass of a string falls into an energy region, the string is identified with the baryon of that mass and no longer allowed to decay. The incident nucleons are taken to be a distribution of string solutions, with the distribution determined [12] from the experimentally measured nucleon structure function. The gluon content of the nucleon is also included by adding gluonic strings where the distribution of string shapes is determined by the gluonic structure function. The interaction between quarks and gluons is also generalized to include a hard component, taken from perturbative QCD, and a soft component, determined phenomenologically from  $e^+e^-$  and  $p$ - $p$  collisions. The partons interact via the hard (soft) interaction if their center-of-mass energy is above (below) a chosen threshold. In addition, we allow the quarks which are created by a string breaking to interact with each other if they are within an interaction radius when they come on-shell.

There are a limited number of parameters in the model, and all are determined from  $e^+e^-$  and  $p$ - $p$  data. These are given in Tables I and V. The model is completely predictive at the  $p$ - $A$  and  $A$ - $A$  level. We present here the first calculations of the extended model. For  $e^+e^-$  and  $p$ - $p$  collisions we find excellent results. This is partially because we adjust our parameters to fit this data. However, we find that over the energy range we examined, the limited number of energy-independent parameters used does reproduce well a broad range of data. We then calculate results for  $p$ - $A$  and  $A$ - $A$  collisions at CERN energies. On the whole, the results are quite satisfactory. The predictions generally lie within the experimental error bars with a few points lying just outside the error bars, as would be expected. We see perhaps more stopping in the data than is produced by the DSP model and an indication of additional transverse momentum production in the  $S + S$  collision.

There is considerable work to be done with the model. The model can predict the energy dependence of distributions measured in  $A$ - $A$  collisions. Predictions of these quantities up to and including RHIC energies are possible. A comparison with the data that will soon be coming forth from RHIC will provide insight into the dynamics of these complex collisions. We have calculated only several measured distributions. There are a number of other quantities which are both measurable and are calculable by the DSP model. We expect that the model will need further refinement as more detailed properties of the reaction are confronted. Finally, a distinct advantage of the model is that it is dynamic; the reaction is generated as a function of time on the computer. This allows us to track in detail the time evolution of important aspects of the reaction, such as the central energy density or the flow of energy or matter. Understanding the time evolution of the reaction can provide great insight on the origin of the asymptotic properties that are to be experimentally measured.

The ultimate goal of relativistic heavy-ion research is to discover and investigate the quark gluon plasma. This will to a great extent be an exercise in understanding the differences between model predictions and data. It is thus very important to constrain the models. In the DSP model, the constraints come from  $e^+e^-$ ,  $p$ - $p$ , and  $p$ - $A$  data. There



exists a limited amount of data for the  $p-p$  and  $p-A$  reactions and this data has reasonably large errors. Future data on these reactions would provide additional constraints on the DSP model as well as other models.

## ACKNOWLEDGMENTS

The work of DEM, ASU, and DJE was supported in part by the US Department of Energy under grant DE-FG02-96ER40975. Oak Ridge National Laboratory is managed by UT-Battelle, LLC for the US Department of Energy under Contract No. DE-AC05-00OR22725.

- 
- [1] Proc. of Quark Matter '99, ed. by L. Riccati, M. Masera and E. Vercellin (North-Holland, New York, 1999).
  - [2] D. J. Dean, Ph.D. thesis, Vanderbilt University (1991) (unpublished).
  - [3] D. J. Dean, A. S. Umar, J.-S. Wu and M. R. Strayer, Phys. Rev. C **45**, 400 (1992).
  - [4] D. J. Dean, M. Gyulassy, B. Müller, E. A. Remler, M. R. Strayer, A. S. Umar and J.-S. Wu, Phys. Rev. C **46**, 2066 (1992).
  - [5] D. J. Dean, A. S. Umar and M. R. Strayer, Phys. Rev. C **48**, 2433 (1993); D. J. Dean, A. S. Umar, and M. R. Strayer, Intl. Jour. of Mod. Phys. E **2**, 565 (1993).
  - [6] X. Artru and G. Mennessier, Nucl. Phys. **B70**, 93 (1974); P. Goddard, J. Goldstone, C. Rebbi, and C. Thorn, Nucl. Phys. **B56**, 109 (1973); T. Goto, Prog. Theo. Phys. **46**, 1560 (1971).
  - [7] B. Andersson, G. Gustafson, G. Ingelman and T. Sjostrand, Phys. Rep. **97**, 33 (1983);
  - [8] B. Andersson, G. Gustafson and B. Nilsson-Almquist, Nucl. Phys. B **281**, 289 (1987); B. Nilsson-Almquist and E. Stenlund, Computer Phys. Comm. **43**, 387 (1987).
  - [9] H. Sorge, H. Stöcker, and W. Greiner, Nucl. Phys. A **498**, 567c (1989); Ann. Phys. **192**, 266 (1989); S.A. Bass *et al.*, Prog. Part. Nucl. Phys. **41**, 255 (1998); S. Scherer *et al.*, Prog. Part. Nucl. Phys. **42**, 279 (1999).
  - [10] N. S. Amelin *et al.*, Phys. Rev. Lett. **67**, 1523 (1991).
  - [11] D. E. Malov, A. S. Umar, D. J. Ernst, and D. J. Dean, Intl. J. Mod. Phys. E **8**, 299 (1999).
  - [12] D. E. Malov, A. S. Umar, D. J. Ernst, and D. J. Dean, Phys. Rev. C **59**, 2289 (1999).
  - [13] G.S. Bali *et al.*, Phys.Rev. D **56**, 2566 (1997); G.S. Bali *et al.*, Phys.Rev. D **55**, 5309 (1997).
  - [14] H. W. Fricke and C. C. Noack, Phys. Rev. Lett. **80**, 3014 (1998).
  - [15] D. E. Malov, Ph.D. thesis, Vanderbilt University (1999) (unpublished).
  - [16] J. D. Bjorken, Phys. Rev. D **27**, 140 (1983).
  - [17] N. K. Glendenning and T. Matsui, Phys. Rev. D **28**, 2890 (1983).
  - [18] K. Sailer, Th. Schönfeld, A. Schäfer, B. Müller, and W. Greiner, (University of Frankfurt preprint UFTP 244/1990).
  - [19] D. J. Ernst, D. E. Malov, and A. S. Umar, Heavy Ion Physics (Proceedings of the III Latin American Workshop on Nuclear and Heavy Ion Physics), in press.
  - [20] D. Perkins, *High Energy Physics*, (Addison-Wesley, 1982), 294.

- [21] M. Althoff *et al.*, TASSO Collaboration, Z. Phys. C **22**, 307 (1984); R. Brandelik *et al.*, TASSO Collaboration, Phys. Lett. **170B**, 290 (1981).
- [22] F. Close, *Quarks and Partons*, (Academic Press, 1981), 171.
- [23] H. L. Lai *et al.*, Phys. Rev. D **55**, 1280 (1997).
- [24] F. Abe *et al.*, Phys. Rev. Lett. **77**, 438 (1996).
- [25] A. Breakstone, *et al.*, Phys. Rev. D **30**, 528 (1984).
- [26] M. E. Peskin, D. V. Schroeder, *An introduction to Quantum Field Theory*, (Addison-Wesley, 1995).
- [27] R. Cutler, D.Sivers, Phys. Rev. D **17**, 196 (1978).
- [28] A. DiGiacomo, M. Maggiore, and S. Oleynik, Phys. Lett. B **236**, 199 (1990).
- [29] M. Jacob, Hadron Physics at ISR Energies, Lectures given in the Academic Training Programme of CERN, 1974 .
- [30] A. M. Rossi, *et al.*, Nucl.Phys. B **84**, 269 (1975).
- [31] T. Fujita and J. Hüfner, Phys. Rev. D **37**, 604 (1989); C. Wong, R. Wang, and C. Shih, Phys. Rev. D **44**, 679 (1991).
- [32] A. K. Kerman, T. Matsui, and B. Svetitsky, Phys. Rev. Lett. **56**, 219 (1986); G. Gatoff, A. K. Kerman, and T. Matsui, Phys. Rev. D **36**, 114 (1987).
- [33] J. Schwinger, Phys. Rev. **82**, 664 (1951); J. Schwinger, Phys. Rev. **128**, 2425 (1962); A. Casher, H. Newberger, and S. Nussinov, Phys. Rev. D **20**, 179 (1979).
- [34] L. P. Csernai, *Introduction to Relativistic Heavy Ion Collisions*, (Jhon Wiley & Sons, 1994), 284.
- [35] L. Bergmann, C. Schaefer, *Constituents of Matter*, (Walter de Gruyter, 1997), 653.
- [36] A. Barton, *et al.*, Phys. Rev. D **26**, 1497 (1982).
- [37] G. A. Miller, e-print, nucl-th/9707040.
- [38] L. Van Hove, Z. Phys. C **21**, 93 (1984).
- [39] C. De Marzo, *et al.*, Phys. Rev. D **26**, 1019 (1982); C. De Marzo, *et al.*, Phys. Rev. D **29**, 2476 (1984).
- [40] Z. Koba, N.B. Nielsen, and P. Olesen, Nucl. Phys. B **40**, 317 (1972).
- [41] T. Alber, *et al.*, NA35 Collaboration, e-print, hep-ex/9711001; T. Alber, *et al.*, Z.Phys. C **64**, 195 (1994); J. Bächler, *et al.*, NA35 Collaboration, Z.Phys. C **52**, 239 (1992).
- [42] J. Bächler, *et al.*, NA35 Collaboration, Phys. Rev. Lett. **72**, 1419 (1994).
- [43] The data from Ref. [41] also include a point at the incident target rapidity. This point is not a directly measured point but is inferred from the data to account for nucleons from the target that do not participate in the reaction but continue on with the incident momentum. We have not performed such an analysis and thus do not include this point in our figures.
- [44] H. Boggild, *et al.*, NA44 Collaboration, e-print, nucl-ex/9808002.
- [45] J. W. Cronin, *et al.*, Phys. Rev. D **11**, 3105 (1975).
- [46] T. Akesson, *et al.*, Z.Phys. C **46**, 361 (1990).
- [47] H Appelshäuser, *et al.*, NA49 Collaboration, Phys. Rev. Lett. **82**, 2471 (1999); J. Bächler, *et al.*, NA49 Collaboration, Nucl. Phys. **A661**, 45c (1999).